research communications

A study of the crystal structures, supramolecular patterns and Hirshfeld surfaces of bromide salts of hypoxanthine and xanthine

Udhayasuriyan Sathya,[a] Jeyaraman Selvaraj Nirmalram,[a]* Sundaramoorthy Gomathi,[b] Durairaj Dhivya,[a] Samson Jegan Jennifer[c] and Ibrahim Abdul Razak[c]

[a]Centre for Research and Development, PRIST Deemed to be University, Thanjavur, 613 403, Tamil Nadu, India, [b]Department of Chemistry, Periyar Maniammai Institute of Science and Technology, Thanjavur 613 403, Tamil Nadu, India, and [c]X-ray Crystallography Unit, School of Physics, University Sains Malaysia, 11800, USM, Penang, Malaysia. *Correspondence e-mail: nirmalramjs@gmail.com
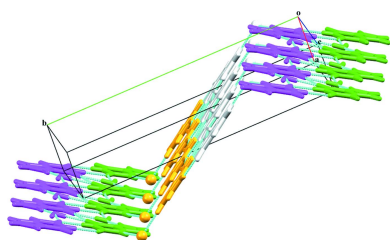
Two new crystalline salts, namely, hypoxanthinium bromide monohydrate, $C_5H_5N_4O^+ \cdot Br^- \cdot H_2O$ (**I**) and xanthinium bromide monohydrate, $C_5H_5N_4O_2^+ \cdot Br^- \cdot H_2O$ (**II**), were synthesized and characterized by single-crystal X-ray diffraction technique and Hirshfeld surface analysis. The hypoxanthinium and xanthinium cations in salts **I** and **II** are both in the oxo-N(9)–H tautomeric form. The crystal packing of the two salts is governed predominantly by N–H···O, N–H···Br, C–H···Br and O–H···Br interactions described by $R_3^2(9)$ and $R_2^2(8)$ synthons. The crystal packing is also consolidated by carbonyl···π interactions between symmetry-related hypoxanthinium (**HX$^+$**) cations in salt **I** and xanthinium cations (**XA$^+$**) in salt **II**. The combination of all these interactions leads to the formation of wave- and staircase-like architectures in salts **I** and **II**, respectively. The largest contributions to the overall Hirshfeld surface are from Br···H/H···Br contacts (22.3% in **I** and 25.4% in **II**).
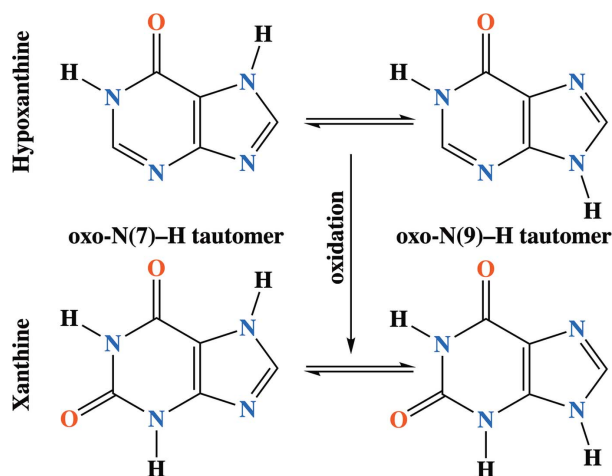
1. Chemical context

Over the past several decades, non-covalent interactions have been found to play a prominent role in coordination chemistry, materials science and pharmaceutical science (Černý & Hobza, 2007; Desiraju, 2013; Perumalla & Sun, 2014). Understanding the role of non-covalent interactions is important in the context of crystal engineering (Aakeröy *et al.*, 2010; Pogoda *et al.*, 2018; Cavallo *et al.*, 2016; Desiraju *et al.*, 2013) in order to design solids with desired properties. When it comes to pharmaceutics, active pharmaceutical ingredients (APIs) are known to exist in different solid forms such as salts, co-crystals, solvates, polymorphs and amorphous solids (Aaltonen *et al.*, 2009). The salt and co-crystal forms of APIs have improved their solubility and bioavailability when compared to pure APIs (Thackaberry, 2012; Xu, *et al.*, 2014). Drugs with low solubility/bioavailability are usually converted to their salts or crystallized in their co-crystal/polymorphic/ solvate forms to enhance their properties. Herein, we report two new salts of hypoxanthine (**HX**) and xanthine (**XA**).

Hypoxanthine ($C_5H_4N_4O$) [systematic name: 1,9-dihydro-purine-6-one] and xanthine ($C_5H_4N_4O_2$) [systematic name: 3,7-dihydro-purine-2,6-dione] are well-known purine-based nucleotides (Emel'yanenko *et al.*, 2017) present in *t*-RNA and DNA in the form of the nucleoside inosine (Plekan *et al.*, 2012). Purine derivatives are widely known for their therapeutic applications such as antagonization of the adenosine
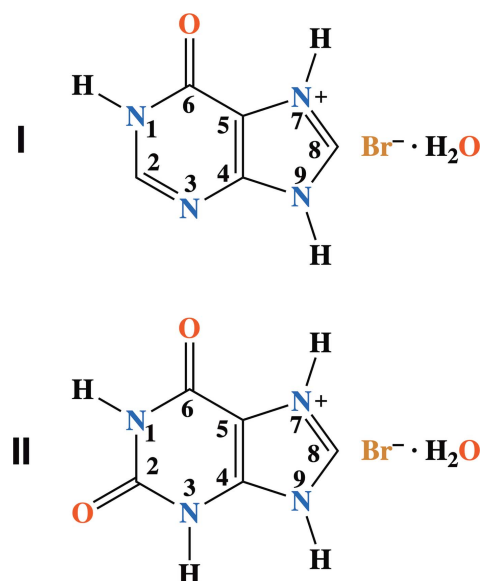
receptor, anti-inflammatory, antimicrobial, antioxidant, anti-tumour, anti-asthmatic and psycho-stimulant drug activity (Meskini *et al.*, 1994; Burbiel *et al.*, 2006). **HX** and **XA** are also found as intermediates in the biological degradation of nucleic acid to uric acid. Furthermore, **HX** is used as an indicator of hypoxia and it is known to inhibit the effect of several drugs (Dubler *et al.*, 1987*a*,*b*). It is also used to destroy harmful agents such as cancer cells (Susithra *et al.*, 2018). Purine-based derivatives of **HX** and **XA** bind with the DNA base pairs through weak hydrogen bonds (Latosińska *et al.*, 2014; Rutledge *et al.*, 2007). Additionally, hypoxanthine-guanine phosphoribosyl transferase plays an important role in activating antiviral drugs in the human body and xanthine has been used as a mild stimulant drug (Faheem *et al.*, 2020).

The structure of hypoxanthine and xanthine consists of fused six-membered pyrimidine and five-membered imidazole rings. **HX** and **XA** can exist in two tautomeric forms, oxo-N(7)–H and oxo-N(9)–H (Plekan *et al.*, 2012; Gulevskaya & Pozharskii, 1991), as shown below. So far, two polymorphic forms of **HX** (Schmalle *et al.*, 1988; Yang & Xie, 2007) and a limited number of hypoxanthinium and xanthinium salts have been reported in the literature; hypoxanthinium nitrate monohydrate, hypoxanthinium chloride monohydrate (Cabaj *et al.*, 2019; Schmalle *et al.*, 1990; Sletten & Jensen, 1969), xanthinium nitrate monohydrate and xanthinium hydrogensulfate monohydrate (Sridhar, 2011).

In the hypoxanthinium salts, the hypoxanthine molecule is usually also protonated at the N7 position, resulting in the oxo-N(9)–H tautomer. Similarly, xanthinium nitrate monohydrate, xanthinium hydrogensulfate monohydrate (Sridhar, 2011) and xanthinium perchlorate dihydrate (Biradha *et al.*, 2010) are also in the oxo-N(9)–H tautomeric form and are therefore protonated on the N7 position. Studies of non-covalent interactions involving hypoxanthine and xanthine bases with inorganic acids have increased because their hydrogen-bonding patterns are similar to those of purine bases (Maixner & Zachova, 1991; Sridhar, 2011; Kistenmancher & Shigematsu, 1974). In the current work, the crystal structures, supramolecular packing patterns and Hirshfeld surface analyses of hypoxanthinium bromide monohydrate (**I**) and xanthinium bromide monohydrate (**II**) are reported.

2. Structural commentary

Hypoxanthinium bromide monohydrate (**I**) crystallizes in the monoclinic space group $P2_1/c$ with one hypoxanthinium cation (**HX**⁺), one bromide anion (**Br**⁻) and one water molecule in the asymmetric unit, as shown in Fig. 1. Here, the **HX**⁺ cation exists in the oxo-N(9)–H tautomeric form with the N7 atom of the purine ring protonated, as can be seen from the N—C bond distance [N7—C8 = 1.3219 (17) Å vs N9—C8 = 1.3419 (18) Å] and C—N—C bond angles [C5—N7—C8 = 107.98 (11)° and C4—N9—C8 = 108.32 (10)°]. Those values are similar to those in the crystal structure of hypoxanthinium chloride monohydrate [N7—C8 = 1.325 (2) Å and N9—C8 = 1.336 (2) Å, C5—N7—C8 = 107.35 (16)° and C4—N9—(C8 = 108.28 (15)°; Kalyanaraman *et al.*, 2007; Sletten & Jensen, 1969]. The N3—C4—C5—N7 and N9—C4—C5—C6 torsion angles are 179.07 (12) and −179.58 (12)°, respectively. These values are similar to those observed in the crystal structure of the neutral hypoxanthine molecule (Schmalle *et al.*, 1988; Yang & Xie, 2007). The **HX**⁺ cation, **Br**⁻ anion and the water
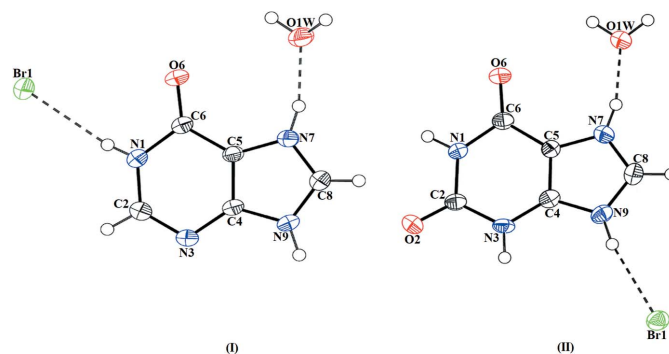

Figure 1
ORTEP view of the molecular components of salts **I** and **II**, showing the atom-labelling scheme. Displacement ellipsoids are drawn at 50% probability level. Hydrogen bonds are shown as dashed lines.

Table 1
Hydrogen-bond geometry (Å, °) for **I**.

$D-H\cdots A$	$D-H$	$H\cdots A$	$D\cdots A$	$D-H\cdots A$
$N9-H9\cdots Br1^{i}$	0.85 (1)	3.08 (2)	3.5397 (12)	117 (2)
$N9-H9\cdots O6^{i}$	0.85 (1)	1.98 (2)	2.7579 (14)	153 (2)
$N1-H1\cdots Br1$	0.84 (1)	2.41 (1)	3.2419 (12)	170 (2)
$N7-H7\cdots O1W^{ii}$	0.85 (1)	1.81 (2)	2.6401 (16)	165 (2)
$O1W-H1W\cdots N3^{iii}$	0.86 (1)	2.08 (1)	2.9200 (16)	165 (2)
$O1W-H2W\cdots Br1$	0.85 (1)	2.48 (1)	3.2894 (12)	161 (2)
$C8-H8\cdots Br1^{i}$	0.93	2.89	3.4875 (15)	123

Symmetry codes: (i) $x+1, -y+\frac{1}{2}, z-\frac{1}{2}$; (ii) $-x-1, y-\frac{1}{2}, -z+\frac{3}{2}$; (iii) $-x, -y+1, -z+1$.

molecule interact through N—H···Br, N—H···O and C—H···Br hydrogen bonds with donor–acceptor distances N···Br = 3.2419 (13) Å, N9···O6 = 2.7579 (14) Å and C8···Br1 = 3.4875 (15) Å (Table 1), forming an $R_3^2(9)$ motif. The water molecule present in the lattice prevents the formation of base pairs (Varani & McClain, 2000) between the **HX⁺** cations.

Xanthinium bromide monohydrate (**II**) also crystallizes in the monoclinic space group $P2_1/c$ with one xanthinium cation (**XA⁺**), one bromide anion (**Br⁻**) and one water molecule in the asymmetric unit (Fig. 1). The **XA⁺** cation has the N7—C8 bond [1.312 (5) Å] shorter than N9–C8 one [1.344 (5) Å]. The C—N—C bond angles are C5—N7—C8 = 108.2 (3)° and C4—N9—C8 = 107.7 (3)° and, therefore, the cation can also be described as the oxo-N(9)–H tautomer. These values are similar to those in xanthinium perchlorate dihydrate [N7—C8 = 1.314 (3) Å, N9—C8 = 1.341 (3) Å, C5—N7—C8 = 108.3 (16)° and C4—N9—C8 = 107.58 (15)°; Biradha et al., 2010). The N3—C4—C5—N7 and N9—C4—C5—C6 torsion angles in **II** are 179.07 (12)° and −179.58 (12)°, respectively. Finally, the two symmetry-related **XA⁺** cations in **II** form a base pair similar to that observed between guanine and uracil (Varani & McClain, 2000).

Figure 3
A view of three-dimensional wave-like supramolecular architecture along the *b*-axis direction.

3. Supramolecular features

In **I**, the protonated **HX⁺** cation interacts with another inversion-related **HX⁺** and **Br⁻** pair via N1—H1···Br1, C8—H8···Br1ⁱⁱ and N9—H9···O6ⁱⁱ hydrogen bonds (Table 1). These interactions lead to the formation of a nine-membered ring with $R_3^2(9)$ (type **D**) primary graph-set motif (Sletten & Jensen, 1969). Along with this, the **HX⁺** cation interacts with another inversion-related **HX⁺** cation and a water molecule through O1W—H1W···N3ⁱⁱⁱ and N7—H7···O1Wⁱⁱ hydrogen bonds. The combination of these interactions leads to the formation of an eleven-membered $R_3^3(11)$ (type **I**) ring motif. The interaction is very similar to the water-mediated base pairs observed in the crystal structure of hypoxanthinium chloride and the nucleobase pairs in DNA and RNA (Sletten & Jensen, 1969; Reddy et al., 2001; Brandl et al., 2000). Here the O1W atom of the water molecule acts as both a hydrogen-bond donor and a hydrogen-bond acceptor. The $R_2^2(9)$ and $R_3^3(11)$ ring motifs combine to form a supramolecular ribbon. Adjacent ribbons are connected through pairs of O1W—H2W···Br1 hydrogen bonds with $R_6^4(16)$ and $R_6^4(14)$ (types **N**
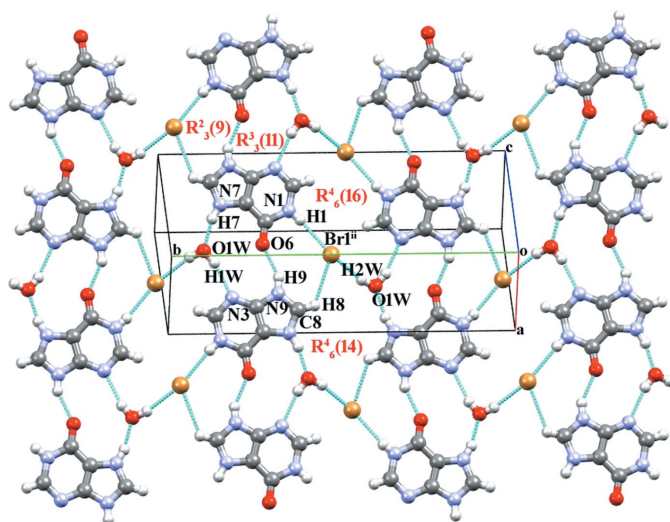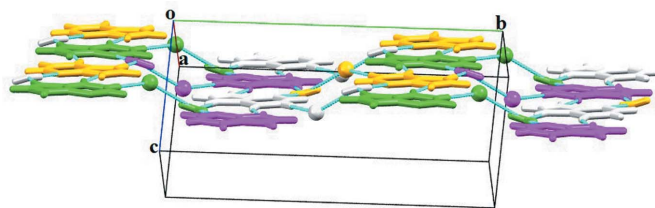

Figure 2
Hypoxanthinium and bromide ions in salt **I** forming ribbons together with water molecules through O—H···Br, N—H···Br and C—H···Br interaction. [Symmetry codes: (i) $-1-x, -\frac{1}{2}+y, \frac{3}{2}-z$; (ii) $1+x, \frac{1}{2}-y, -\frac{1}{2}+z$; (iii) $-x, 1-y, 1-z$].
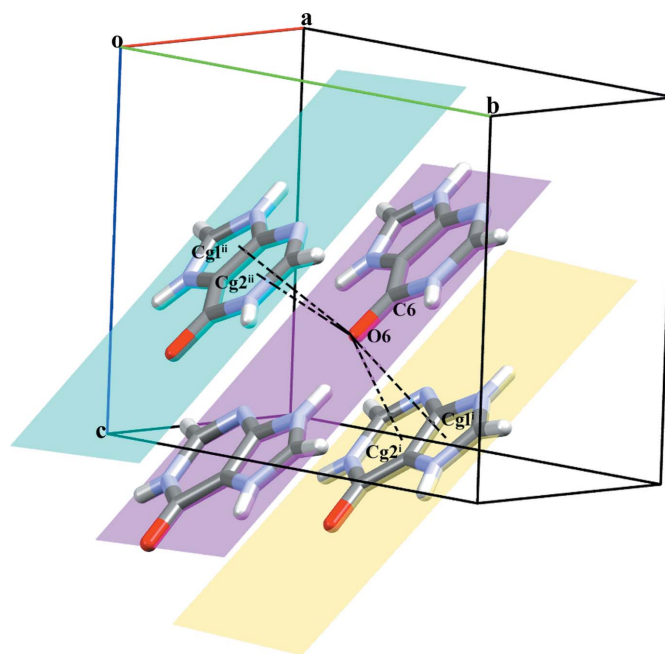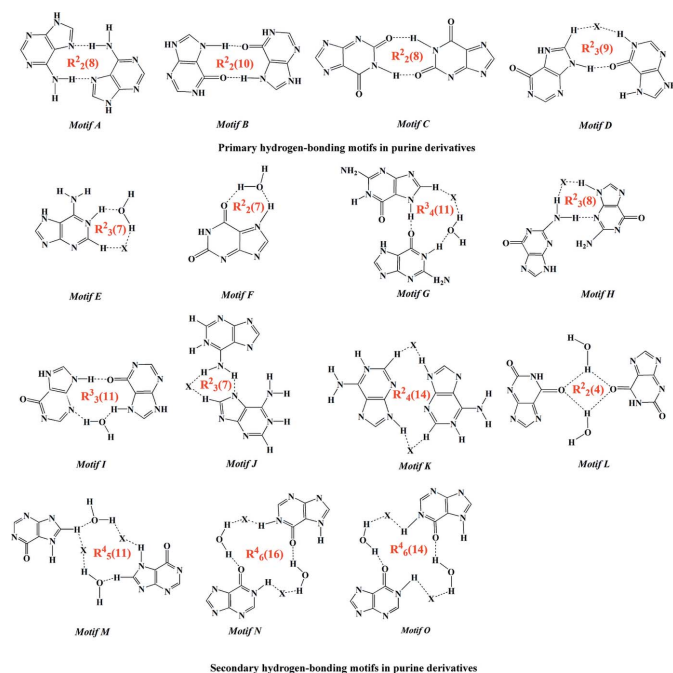

Figure 4
A view of the C=O(carbonyl)···π interactions (dashed lines) between the **HX⁺** cations in salt **I**. [Symmetry codes: (i) $-1+x, y, z$; (ii) $x, \frac{1}{2}-y, \frac{1}{2}+z$].

Table 2
Hydrogen-bond geometry (Å, °) for **II**.

D—H$\cdots A$	D—H	H$\cdots A$	$D\cdots A$	D—H$\cdots A$
N1—H1$\cdots$O2^i	0.82 (2)	2.09 (2)	2.903 (4)	175 (4)
N3—H3$\cdots$Br1^{ii}	0.82 (2)	2.48 (2)	3.301 (3)	176 (4)
N7—H7$\cdots$O1W	0.82 (2)	1.81 (2)	2.609 (4)	163 (4)
N9—H9$\cdots$Br1	0.82 (2)	2.43 (2)	3.237 (3)	172 (4)
O1W—H1$WA\cdots$O6^{iii}	0.86 (1)	1.95 (1)	2.802 (4)	171 (5)
O1W—H1$WB\cdots$Br1^{iv}	0.86 (1)	3.03 (4)	3.490 (3)	115 (3)
O1W—H1$WB\cdots$O2^v	0.86 (1)	2.05 (3)	2.816 (4)	149 (4)

Symmetry codes: (i) $-x+1, -y+1, -z+2$; (ii) $x, -y+\frac{1}{2}, z+\frac{1}{2}$; (iii) $-x+2, -y+1, -z+1$; (iv) $x+1, -y+\frac{1}{2}, z-\frac{1}{2}$; (v) $x+1, y, z-1$.

and O motifs) ring motifs, respectively, through pairs of C8—H8$\cdots$Br1^i and N7—H7$\cdots$O1W^{ii} hydrogen bonds (Fig. 2). The combination of all these interactions leads to the formation of a wave-like supramolecular architecture that extends along the b-axis direction (Fig. 3). The crystal structure is further consolidated by carbonyl$\cdots\pi$ interactions (C6=O6 and π cloud of the imidazole (centroid $Cg1$) and pyridine (centroid $Cg2$) rings of the **HX$^+$** cation) between symmetry-related cations with C=O$\cdots Cg1^{iv}$, C=O$\cdots Cg1^v$, C=O$\cdots Cg2^{iv}$ and C=O$\cdots Cg2^v$ distances of 3.5796 (12), 3.2478 (12) Å, 3.3862 (12) and 3.4747 (12) Å, respectively, and angles of 101.58 (8), 91.45 (8), 105.03 (8) and 103.46 (8)°, respectively [symmetry codes: (iv) $-1 + x, y, z$; (v) $x, \frac{1}{2} - y, \frac{1}{2} + z$] (Fig. 4). Salt **I** is isomorphous with hypoxanthinium chloride monohydrate (Sletten & Jensen, 1969).

Motif A — $R_2^2(8)$
Motif B — $R_2^2(10)$
Motif C — $R_2^2(8)$
Motif D — $R_3^2(9)$

Primary hydrogen-bonding motifs in purine derivatives

Motif E — $R_3^2(7)$
Motif F — $R_2^2(7)$
Motif G — $R_4^2(11)$
Motif H — $R_3^2(8)$

Motif I — $R_3^3(11)$
Motif J — $R_3^2(7)$
Motif K — $R_4^2(14)$
Motif L — $R_2^2(4)$

Motif M — $R_5^4(11)$
Motif N — $R_6^4(16)$
Motif O — $R_6^4(14)$

Secondary hydrogen-bonding motifs in purine derivatives

In the crystal structure of salt **II**, the **XA$^+$** cation interacts with its inversion-related equivalent to form a dimer through a pair of N1—H1$\cdots$O2^i hydrogen bonds (Table 2) with an $R_2^2(8)$ graph-set motif (type **C** in the scheme above). The dimer is flanked on both sides by a water molecule (O1W), forming a pair of O1W—H2$W\cdots$O2^{iv} and O1W—H1$W\cdots$O6^{ii} hydrogen bonds with an $R_3^2(8)$ graph-set motif (type **H**), leading to the formation of a tetrameric unit. The tetrameric unit is formed
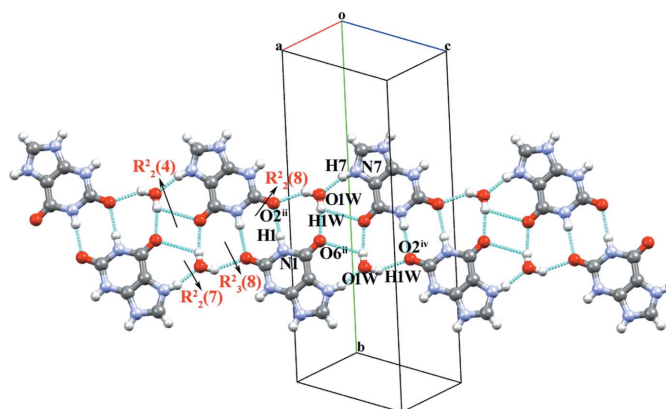

Figure 5
Formation of a supramolecular ribbon with a *DADA* array in salt **II** *via* N—H$\cdots$O and O—H$\cdots$O hydrogen bonds between cations and water molecules.

by an alternate arrangement of $R_2^2(8)$ and $R_3^2(8)$ ring motifs, which extend as *DADA* array (dimeric units held together by four hydrogen bonds between the self-complementary *DADA* arrays; D = donor and A = acceptor) along the ac plane. Neighbouring tetrameric units are then connected through two sets of $R_2^2(7)$ motifs (Jeffrey & Saenger, 1991) formed by N7—H7$\cdots$O1W and O1W—H1$W\cdots$O6^{ii} hydrogen bonds and an $R_2^2(4)$ (type **L**) motif formed by a pair of O1W—H1$W\cdots$O6^{ii} interactions. The tetrameric units combine into a supramolecular ribbon extended along the ac plane (Fig. 5). Neighbouring perpendicular supramolecular ribbons are then interconnected through pairs of N3—H3$\cdots$Br1^{iii} and N9—H9$\cdots$Br1 hydrogen bonds with an $R_8^6(28)$ ring motif, which assembles them into a staircase-like supramolecular architecture as shown in Figs. 6 and 7. The crystal structure is further consolidated by carbonyl$\cdots\pi$ interactions between symmetry-related **XA$^+$** cations [C6=O6 and π cloud of the pyridine ring (centroid $Cg2$) of the **XA$^+$** unit) with C=O$\cdots Cg2^{vi}$ and C=O$\cdots Cg2^{vii}$ distances of 3.366 (3) and 3.477 (3) Å, respectively, and angles of 108.2 (2) and 118.7 (2)° [symmetry codes: (vi) $1 + x, y, z$; (vii) $1 - x, 1 - y, 1 - z$; Fig. 8].
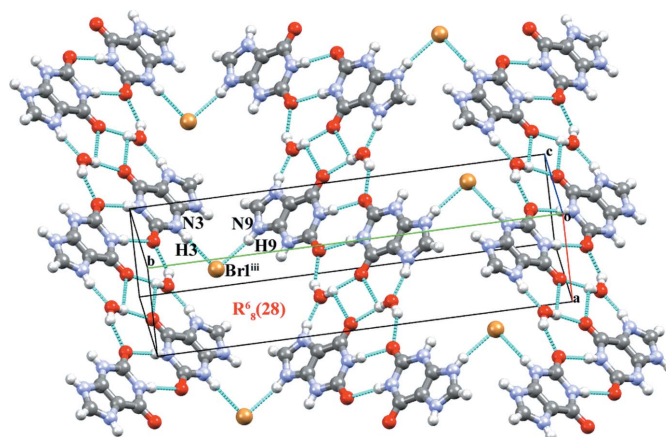

Figure 6
Supramolecular ribbons connecting adjacent ribbons through N—H$\cdots$Br interactions. [Symmetry codes: (i) $1 - x, 1 - y, 2 - z$; (ii) $2 - x, 1 - y, 1 - z$; (iii) $x, \frac{1}{2} - y, \frac{1}{2} + z$; (iv) $1 + x, y, -1 + z$.]
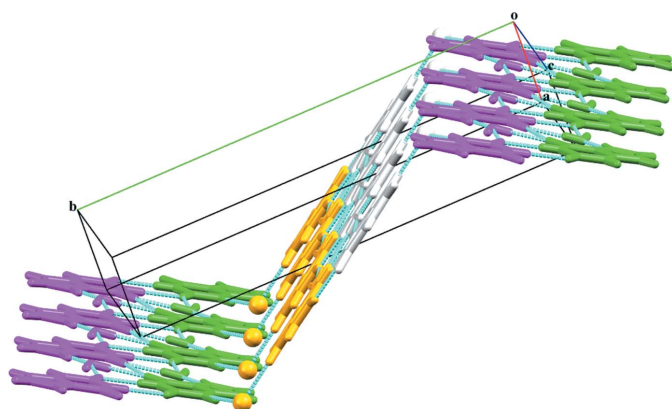
Figure 7
The formation of a three-dimensional supramolecular staircase structure along the *ac* plane.

4. Hirshfeld surface analysis

Hirshfeld surface analyses and their associated two-dimensional fingerprint plots (McKinnon *et al.*, 2007; Spackman & Jayatilaka, 2009) were generated using *Crystal Explorer 17.5* (Turner *et al.*, 2017). The Hirshfeld surfaces of the title compounds mapped over d_{norm} feature several red spots in the regions of *D–A* (*D* = donor, *A* = acceptor) interactions (Cárdenas-Valenzuela *et al.*, 2018; Atioğlu *et al.*, 2018). In this regard, the contribution of the interatomic contacts to the d_{norm} surface map can help differentiate whether the contact is longer (blue) or shorter (red) than the sum of the van der Waals radii of the two interacting atoms. The Hirshfeld surfaces of salts **I** and **II** are shown in Fig. 9*a* and 10*a*, respectively and the hydrogen-bonding interactions between the hydrated ion pairs **I** and **II** and the respective neighbouring moieties are shown in Fig. 9*b* and 10*b*, respectively. The intense red spots on the Hirshfeld surface indicate the
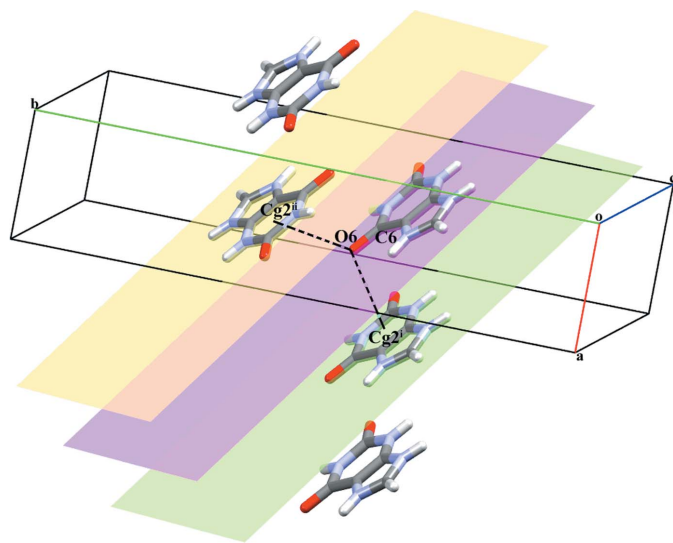

Figure 8
A view of the C=O(carbonyl)···π interactions between **XA⁺** cations in salt **II**. [Symmetry codes: (i) 1 + x, y, z; (ii) 1 − x, 1 − y, 1 − z].

Figure 9
(*a*) Hirshfeld surface mapped over d_{norm} for salt **I**. (*b*) Intermolecular interactions and the three-dimensional Hirshfeld surface for salt **I**.

shortest interatomic distances corresponding to the hydrogen bonds. They are also clearly identified by the two long spikes in the fingerprint plots and can be quantified using the percentage distribution of the interacting types. Such analyses of the salts **I** and **II** are shown in Figs. 11 and 12 giving the following contributions: All (100%), O···H/H···O (**I** 19.7%, **II** 23.4%), N···H/H···N (**I** 13.5%, **II** 7.5%) C···H/H···C (**I** 6.4%, **II** 9.6%), H···H/H···H (**I** 23.4%, **II** 15.9%) and C···C/C···C (**I** 0.9%, **II** 0.1%) (Table 5), indicating that the most abundant contact is Br···H/H···Br with 22.3% in **I** and 25.4% in **II**, respectively.

5. Comparative analysis

The data obtained by comparative analysis of the crystal structures, supramolecular interactions, hydrogen-bonding motifs and packing patterns of structurally similar halide salts such as adeninium bromide, adeninium chloride, guaninium bromide, guaninium chloride and hypoxanthinium chloride (Maixner & Zachova, 1991; Sridhar, 2011; Kistenmancher & Shigematsu, 1974; Langer & Huml, 1978) are listed and compared in Table 3.

Salt **I** has similar unit-cell parameters and packing patterns to the hypoxanthinium chloride salt. The molecular recognition between the hypoxanthine base and acid happens *via* N—H···O, C—H···Br/Cl and N—H···Br/Cl hydrogen-bond motifs with $R_3^2(9)$ (type ***D***), $R_3^3(11)$ (type ***I***), $R_6^4(16)$ (type ***N***) and $R_6^4(14)$ (type ***O***) graph-set motifs. Salt **II** forms base pairs
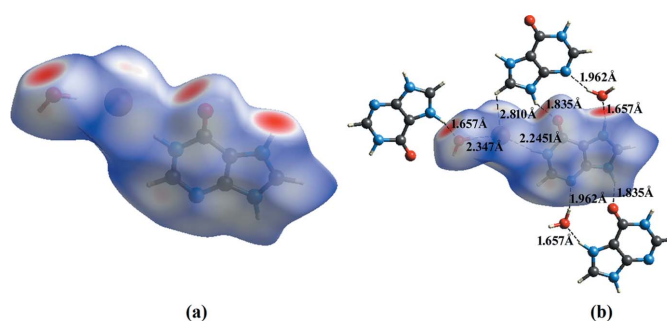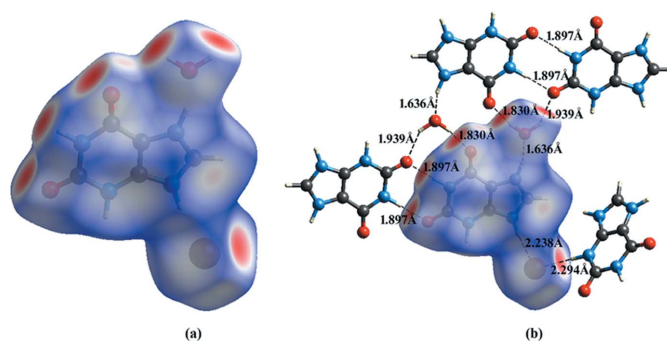

Figure 10
(*a*) Hirshfeld surface mapped over d_{norm} for salt **II**. (*b*) Intermolecular interactions and the three-dimensional Hirshfeld surface for salt **II**.

Table 3
Comparison of purine derivatives with hydrobromic acid and hydrochloric acid.

	Adeninium bromide hemihydrate	Adeninium chloride monohydrate	Guaninium chloride monohydrate	Guaninium bromide monohydrate	Hypoxanthinium chloride monohydrate	Hypoxanthinium bromide monohydrate (**I**)	Xanthinium bromide monohydrate (**II**)
Cell parameters (a, b, c, β; Å, °)	9.018 (2), 4.845 (2), 19.693 (5), 112.8	8.771 (2), 4.834 (2), 19.46 (1), 114.25	4.591 (1), 9.886 (2), 18.985 (1), 99.62	4.8708 (7), 13.237 (3), 14.638 (2), 93.906 (10)	4.8295 (9), 17.7285 (22), 9.0077 (21), 94.59 (3)	4.8487 (4), 18.4455 (15), 9.0782 (7), 94.808 (1)	4.9225 (2), 22.7572 (17), 7.5601 (5), 103.003 (3)
Crystal system	Monoclinic	Monoclinic	Monoclinic	Monoclinic	Monoclinic	Monoclinic	Monoclinic
Space group	$P2/c$	$P2/c$	$P2_1/c$	$P2_1/c$	$P2_1/c$	$P2_1/c$	$P2_1/c$
Protonation site	N1	N1	N7	N7	N7	N7	N9
Type of hydrogen bonding	N—H⋯O, N—H⋯Br, N—H⋯N, O—H⋯O, C—H⋯Br	N—H⋯O, N—H⋯Cl, N—H⋯N, O—H⋯Cl, C—H⋯Cl	N—H⋯O, N—H⋯Br, N—H⋯N, O—H⋯Br, C—H⋯Br	N—H⋯O, N—H⋯Cl, N—H⋯N, O—H⋯Br, C—H⋯Br	N—H⋯Cl, N—H⋯O, O—H⋯N, O—H⋯Cl, C—H⋯Cl	N—H⋯Br, N—H⋯O, O—H⋯N, O—H⋯Br, C—H⋯Br	N—H⋯O, N—H⋯Br, O—H⋯O
Type of stacking	–	–	C=O⋯π	C=O⋯π	C=O⋯π	C=O⋯π	C=O⋯π
Primary motif	$R_2^2(10)$	$R_2^2(10)$	$R_2^2(8)$	$R_2^2(8)$	$R_3^2(9)$	$R_3^2(9)$	$R_2^2(8)$
Secondary motif	$R_3^2(7)$, $R_4^2(14)$	$R_3^2(7)$, $R_4^2(14)$	$R_3^2(7)$, $R_2^2(10)$, $R_4^3(11)$	$R_3^2(7)$, $R_2^2(10)$, $R_4^3(11)$	$R_3^3(11)$, $R_6^4(16)$, $R_6^4(14)$	$R_3^3(11)$, $R_6^4(16)$, $R_6^4(14)$	$R_2^2(7)$, $R_2^2(4)$
Type of packing architecture	Ribbon	Ribbon	Ribbon	Ribbon	Wave	Wave	Staircase

via N—H⋯O hydrogen bonds described by $R_2^2(8)$ (type ***C***), $R_2^3(8)$ (type ***H***) (Wei, 1977; Maixner & Zachova, 1991), $R_2^2(7)$ (type ***F***) and $R_2^2(4)$ (type ***L***) graph-set motifs. Salt **II** cannot be compared with its chloride analogue since its crystal structure has not yet been reported.

A comparison between some related purine-based chloride and bromide salts revealed that type ***A***, ***B*** and ***C*** hydrogen-bond motifs are predominant. The commonly observed motifs in purine based salts are shown in the scheme. A comparison of salts **I** and **II** with the reported crystal structures revealed that the bromide and chloride salts of **I** are isomorphous and therefore, one might predict, the unreported xanthinium chloride monohydrate could be isomorphous with its bromide salt **II**.

6. Database survey

A survey of the Cambridge Structural Database (CSD, version 5.43, update of March 2022; Groom *et al.*, 2016) for reported structures of hypoxanthine and xanthine derivatives identified the hypoxanthine molecule (CSD refcodes GEBTUC and GETBUC01; Schmalle *et al.*, 1988; Yang & Xie, 2007) and the following salts: hypoxanthinium nitrate monohydrate (BONKOE and BONKOE54; Cabaj *et al.*, 2019; Schmalle *et al.*, 1990), hypoxanthinium chloride monohydrate (HYPXCL and HYPXCL01; Sletten & Jensen, 1969; Kalyanaraman *et al.*, 2007) as well as three xanthine salts, *viz.* xanthinium perchlorate monohydrate (VURMUR; Biradha *et al.*, 2010), xanthinium nitrate monohydrate (YADJAQ; Sridhar, 2011) and xanthinium hydrogensulfate monohydrate (YADJEU; Sridhar, 2011). In all of the hypoxanthinium salts, the hypox-

Figure 11
Hirshfeld surface analysis and two-dimensional fingerprint plots for salt **I** plotted over d_{norm}, with interactions to neighbouring fragments shown as dashed lines.

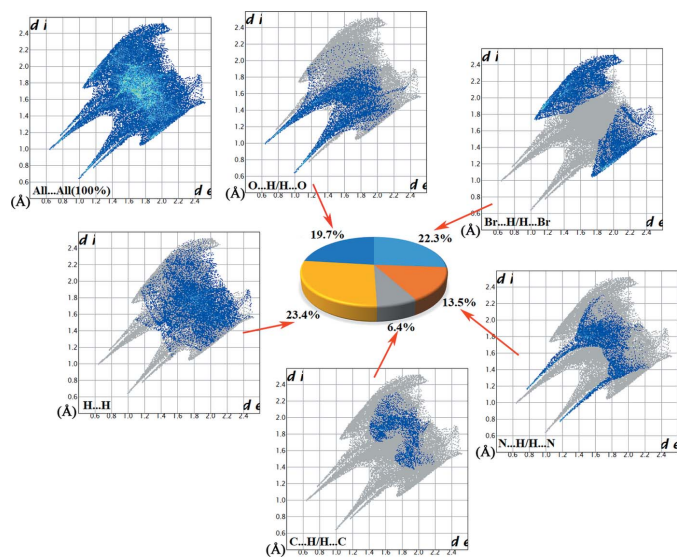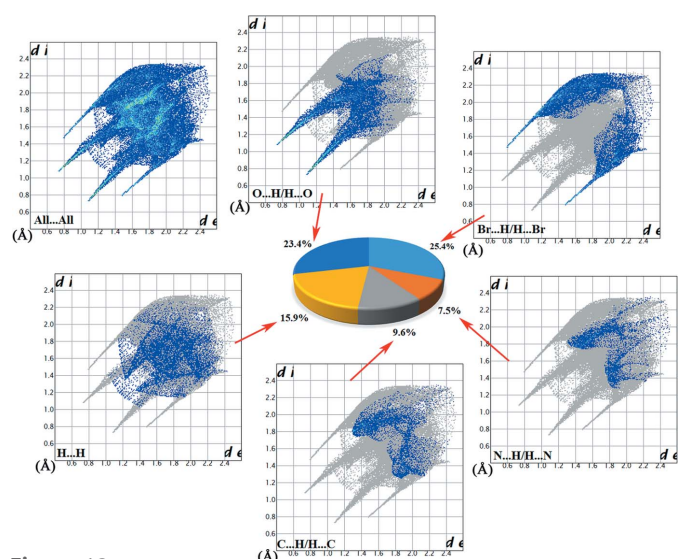
Figure 12
Hirshfeld surface analysis and two-dimensional fingerprint plots for salt **II** plotted over d_{norm}, with interactions to neighbouring fragments shown as dashed lines.

Table 4
Experimental details.

	I	II
Crystal data		
Chemical formula	$C_5H_5N_4O^+ \cdot Br^- \cdot H_2O$	$C_5H_5N_4O_2^+ \cdot Br^- \cdot H_2O$
M_r	235.06	251.06
Crystal system, space group	Monoclinic, $P2_1/c$	Monoclinic, $P2_1/c$
Temperature (K)	296	303
a, b, c (Å)	4.8487 (4), 18.4455 (15), 9.0782 (7)	4.9225 (2), 22.7572 (17), 7.5601 (5)
β (°)	94.808 (1)	103.003 (3)
V (Å^3)	809.07 (11)	825.18 (9)
Z	4	4
Radiation type	Mo $K\alpha$	Mo $K\alpha$
μ (mm^{-1})	5.05	4.96
Crystal size (mm)	$0.46 \times 0.26 \times 0.21$	$0.55 \times 0.37 \times 0.31$
Data collection		
Diffractometer	Bruker APEXII CCD	Bruker APEXII CCD
Absorption correction	Multi-scan (*SADABS*; Bruker, 2016)	Multi-scan (*SADABS*; Bruker, 2016)
T_{min}, T_{max}	0.403, 0.641	0.316, 0.561
No. of measured, independent and observed $[I > 2\sigma(I)]$ reflections	17895, 2383, 2037	5810, 1855, 1418
R_{int}	0.028	0.045
$(\sin\theta/\lambda)_{max}$ (Å^{-1})	0.707	0.696
Refinement		
$R[F^2 > 2\sigma(F^2)]$, $wR(F^2)$, S	0.021, 0.056, 1.05	0.036, 0.080, 1.10
No. of reflections	2383	1855
No. of parameters	128	139
No. of restraints	6	9
H-atom treatment	H atoms treated by a mixture of independent and constrained refinement	Only H-atom coordinates refined
$\Delta\rho_{max}, \Delta\rho_{min}$ (e Å^{-3})	0.34, −0.29	0.42, −0.62

Computer programs: *APEX2* and *SAINT* (Bruker, 2016), *SHELXS97* (Sheldrick 2008), *SHELXT2014/5* (Sheldrick, 2015a), *SHELXL2018/3* (Sheldrick, 2015b), *PLATON* (Spek, 2020), *Mercury* (Macrae *et al.*, 2020), *POVRay* (Cason, 2004) and *publCIF* (Westrip,2010).

anthine molecule is protonated at the N7 position and interacts with the anion through N—H···Cl/O and C=O···π interactions. In the xanthinium salts, the xanthine molecules are protonated at the N7 position in xanthinium nitrate monohydrate and xanthinium hydrogensulfate monohydrate and at the N9 position in xanthinium perchlorate monohydrate. In all of the crystal structures, the xanthinium cation interacts with the anion through N—H···O, O—H···O and C=O···π interactions.

7. Synthesis and crystallization

A general method was used for the preparation and crystallization of the hypoxanthinium bromide monohydrate (**I**) and xanthinium bromide monohydrate (**II**) using the following quantities: 0.0340 mg (0.25mmol) of hypoxanthine for **I** and 0.0380 mg (0.25 mmol) of xanthine for **II**.

The indicated amount of the base was dissolved in 20 mL of distilled water and 2 mL of hydrobromic acid (5% in water) were added. The reaction mixture was heated to 358 K for 30 min using a water bath. The resulting solution was allowed to slowly evaporate at room temperature. After a few days, colourless plate-like crystals were obtained.

8. Refinement

Crystal data, data collection and structure refinement details for salts **I** and **II** are summarized in Table 4. All C-bound

hydrogen atoms were placed in idealized positions and refined using a riding model, with C—H = 0.93 Å and $U_{iso}(H) = 1.2U_{eq}$ (C). The H atoms of the water molecule were located in a difference-Fourier map and refined with the O—H distance restrained to 0.85–0.86 Å and with $U_{iso}(H) = 1.5 U_{eq}(O)$. The hydrogen atoms bound to the nitrogen atoms in salts **I** and **II** were located in difference-Fourier maps and either refined freely (in **I**) or with the distance restraint N—H = 0.82 Å and with $U_{iso}(H) = 1.2U_{eq}(N)$ (in **II**).

References

Aakeröy, C. B., Champness, N. R. & Janiak, C. (2010). *CrystEngComm*, **12**, 22–43.

Aaltonen, J., Allesø, M., Mirza, S., Koradia, V., Gordon, K. C. & Rantanen, J. (2009). *Eur. J. Pharm. Biopharm.* **71**, 23–37.

Atioğlu, Z., Akkurt, M., Toze, F. A. A., Mammadova, G. Z. & Panahova, H. M. (2018). *Acta Cryst.* E**74**, 1035–1038.

Biradha, K., Samai, S., Maity, A. C. & Goswami, S. (2010). *Cryst. Growth Des.* **10**, 937–942.

Brandl, M., Meyer, M. & Sühnel, J. (2000). *J. Phys. Chem. A*, **104**, 11177–11187.

Bruker (2016). *APEX2*, *SADABS* and *SAINT*. Bruker AXS Inc., Madison, Wisconsin, USA.

Burbiel, J. C., Hockemeyer, J. & Muller, C. E. (2006). *Beilstein J. Org. Chem.* **2**, 1–7.

Cabaj, M. K., Gajda, R., Hoser, A., Makal, A. & Dominiak, P. M. (2019). *Acta Cryst.* C**75**, 1036–1044.

Cárdenas-Valenzuela, A. J., González-García, G., Zárraga-Nuñez, R., Höpfl, H., Campos-Gaxiola, J. J. & Cruz-Enríquez, A. (2018). *Acta Cryst.* E**74**, 441–444.

Cason, C. J. (2004). *POV-RAY for Windows*. Persistence of Vision, Raytracer Ptv. Ltd, Victoria, Australia. URL:http://www.povray.org

Cavallo, G., Metrangolo, P., Milani, R., Pilati, T., Priimagi, A., Resnati, G. & Terraneo, G. (2016). *Chem. Rev.* **116**, 2478–2601.

Černý, J. & Hobza, P. (2007). *Phys. Chem. Chem. Phys.* **9**, 5291–5303.

Desiraju, G. R. (2013). *J. Am. Chem. Soc.* **135**, 9952–9967.

Desiraju, G. R., Ho, P. S., Kloo, L., Legon, A. C., Marquardt, R., Metrangolo, P., Politzer, P., Resnati, G. & Rissanen, K. (2013). *Pure Appl. Chem.* **85**, 1711–1713.

Dubler, E., Hänggi, G. & Bensch, W. (1987a). *J. Inorg. Biochem.* **29**, 269–288.

Dubler, E., Hänggi, G. & Schmalle, H. (1987b). *Acta Cryst.* C**43**, 1872–1875.

Emel'yanenko, V. N., Zaitsau, D. H. & Verevkin, S. P. (2017). *J. Chem. Eng. Data*, **62**, 2606–2609.

Faheem, B. K., Kumar, K., Sekhar, K. V. G. C., Kunjiappan, S., Jamalis, J., Balaña-Fouce, R., Tekwani, B. L. & Sankaranarayanan, M. (2020). *Bioorg. Chem.* **104**, 104269–104269.

Groom, C. R., Bruno, I. J., Lightfoot, M. P. & Ward, S. C. (2016). *Acta Cryst.* B**72**, 171–179.

Gulevskaya, A. V. & Pozharskii, A. F. (1991). *Chem. Heterocycl. Compd.* **27**, 1–23.

Jeffrey, J. A. & Saenger, W. (1991). *Hydrogen Bonding in Biological Structures.* Berlin Heidelberg: Springer.

Kalyanaraman, S., Krishnakumar, V. & Ganesan, K. (2007). *Spectrochim. Acta A Mol. Biomol. Spectrosc.* **67**, 750–755.

Kistenmacher, T. J. & Shigematsu, T. (1974). *Acta Cryst.* B**30**, 166–168.

Langer, V. & Huml, K. (1978). *Acta Cryst.* B**34**, 1881–1884.

Latosińska, J. N., Latosińska, M., Seliger, J., Žagar, V. & Kazimierczuk, Z. (2014). *J. Phys. Chem. B*, **118**, 10837–10853.

Macrae, C. F., Sovago, I., Cottrell, S. J., Galek, P. T. A., McCabe, P., Pidcock, E., Platings, M., Shields, G. P, Stevens, J. S., Towler, M. & Wood, P. A. (2020). *J. Appl. Cryst.* **53**, 226–235.

Maixner, J. & Zachová, J. (1991). *Acta Cryst.* C**47**, 2474–2476.

McKinnon, J. J., Jayatilaka, D. & Spackman, M. A. (2007). *Chem. Commun.* pp. 3814–3816.

Meskini, N., Némoz, G., Okyayuz-Baklouti, I., Lagarde, M. & Prigent, A. F. (1994). *Biochem. Pharmacol.* **47**, 781–788.

Perumalla, S. R. & Sun, C. C. (2014). *J. Pharm. Sci.* **103**, 1126–1132.

Plekan, O., Feyer, V., Richter, R., Moise, A., Coreno, M., Prince, K. C., Zaytseva, I. L., Moskovskaya, T. E., Soshnikov, D. Y. & Trofimov, A. B. (2012). *J. Phys. Chem. A*, **116**, 5653–5664.

Pogoda, D., Matera-Witkiewicz, A., Listowski, M., Janczak, J. & Videnova-Adrabinska, V. (2018). *Acta Cryst.* C**74**, 372–380.

Reddy, C., Das, A. & Jayaram, B. (2001). *J. Mol. Biol.* **314**, 619–632.

Rutledge, L. R., Wheaton, C. A. & Wetmore, S. D. (2007). *Phys. Chem. Chem. Phys.* **9**, 497–509.

Schmalle, H. W., Hänggi, G. & Dubler, E. (1988). *Acta Cryst.* C**44**, 732–736.

Schmalle, H. W., Hänggi, G. & Dubler, E. (1990). *Acta Cryst.* C**46**, 340–342.

Sheldrick, G. M. (2008). *Acta Cryst.* A**64**, 112–122.

Sheldrick, G. M. (2015a). *Acta Cryst.* A**71**, 3–8.

Sheldrick, G. M. (2015b). *Acta Cryst.* C**71**, 3–8.

Sletten, J. & Jensen, L. H. (1969). *Acta Cryst.* B**25**, 1608–1614.

Spackman, M. A. & Jayatilaka, D. (2009). *CrystEngComm*, **11**, 19–32.

Spek, A. L. (2020). *Acta Cryst.* E**76**, 1–11.

Sridhar, B. (2011). *Acta Cryst.* C**67**, o382–o386.

Susithra, G., Ramalingam, S., Periandy, S. & Aarthi, R. (2018). *Egypt. J. Basic Appl. Sci.* **5**, 313–326.

Thackaberry, E. A. (2012). *Expert Opin. Drug Metab. Toxicol.* **8**, 1419–1433.

Turner, M. J., MacKinnon, J. J., Wolff, S. K., Grimwood, D. J., Spackman, P. R., Jayatilaka, D. & Spackman, M. A. (2017). *Crystal Explorer17.5.* University of Western Australia. http://hirshfeldsurface.net.

Varani, G. & McClain, W. H. (2000). *EMBO Rep.* **1**, 18–23.

Wei, C. H. (1977). *Cryst. Struct. Commun.* **6**, 525–529.

Westrip, S. P. (2010). *J. Appl. Cryst.* **43**, 920–925.

Xu, Y., Jiang, L. & Mei, X. (2014). *Acta Cryst.* B**70**, 750–760.

Yang, R.-Q. & Xie, Y.-R. (2007). *Acta Cryst.* E**63**, o3309.

supporting information

A study of the crystal structures, supramolecular patterns and Hirshfeld surfaces of bromide salts of hypoxanthine and xanthine

Udhayasuriyan Sathya, Jeyaraman Selvaraj Nirmalram, Sundaramoorthy Gomathi, Durairaj Dhivya, Samson Jegan Jennifer and Ibrahim Abdul Razak

Computing details

For both structures, data collection: *APEX2* (Bruker, 2016); cell refinement: *SAINT* (Bruker, 2016); data reduction: *SAINT* (Bruker, 2016). Program(s) used to solve structure: *SHELXS97* (Sheldrick 2008) for (I); *SHELXT2014/5* (Sheldrick, 2015*a*) for (II). For both structures, program(s) used to refine structure: *SHELXL2018/3* (Sheldrick, 2015*b*); molecular graphics: *PLATON* (Spek, 2020), *Mercury* (Macrae *et al.*, 2020) and *POVRay* (Cason, 2004); software used to prepare material for publication: *PLATON* (Spek, 2020) and *publCIF* (Westrip,2010).

6-Oxo-6,9-dihydro-1*H*-purin-7-ium bromide monohydrate (I)

Crystal data

$C_5H_5N_4O^+ \cdot Br^- \cdot H_2O$	$F(000) = 464$
$M_r = 235.06$	$D_x = 1.930$ Mg m^{-3}
Monoclinic, $P2_1/c$	Mo $K\alpha$ radiation, $\lambda = 0.71073$ Å
$a = 4.8487$ (4) Å	Cell parameters from 2383 reflections
$b = 18.4455$ (15) Å	$\theta = 2.2$–30.2°
$c = 9.0782$ (7) Å	$\mu = 5.05$ mm^{-1}
$\beta = 94.808$ (1)°	$T = 296$ K
$V = 809.07$ (11) Å^3	Plate, colourless
$Z = 4$	$0.46 \times 0.26 \times 0.21$ mm

Data collection

Bruker APEXII CCD diffractometer	2383 independent reflections
φ and ω scans	2037 reflections with $I > 2\sigma(I)$
Absorption correction: multi-scan (SADABS; Bruker, 2016)	$R_{int} = 0.028$
	$\theta_{max} = 30.2°$, $\theta_{min} = 2.2°$
$T_{min} = 0.403$, $T_{max} = 0.641$	$h = -6 \rightarrow 6$
17895 measured reflections	$k = -25 \rightarrow 26$
	$l = -12 \rightarrow 12$

Refinement

Refinement on F^2	Primary atom site location: structure-invariant direct methods
Least-squares matrix: full	Secondary atom site location: difference Fourier map
$R[F^2 > 2\sigma(F^2)] = 0.021$	
$wR(F^2) = 0.056$	Hydrogen site location: mixed
$S = 1.05$	H atoms treated by a mixture of independent and constrained refinement
2383 reflections	
128 parameters	
6 restraints	

$w = 1/[\sigma^2(F_o^2) + (0.0273P)^2 + 0.2516P]$
where $P = (F_o^2 + 2F_c^2)/3$
$(\Delta/\sigma)_{max} = 0.002$
$\Delta\rho_{max} = 0.34$ e Å^{-3}
$\Delta\rho_{min} = -0.29$ e Å^{-3}

Extinction correction: SHELXL2018/3
(Sheldrick 2015b),
$Fc^* = kFc[1+0.001xFc^2\lambda^3/\sin(2\theta)]^{-1/4}$
Extinction coefficient: 0.0080 (9)

Special details

Geometry. All esds (except the esd in the dihedral angle between two l.s. planes) are estimated using the full covariance matrix. The cell esds are taken into account individually in the estimation of esds in distances, angles and torsion angles; correlations between esds in cell parameters are only used when they are defined by crystal symmetry. An approximate (isotropic) treatment of cell esds is used for estimating esds involving l.s. planes.

Fractional atomic coordinates and isotropic or equivalent isotropic displacement parameters (Å^2)

	x	*y*	*z*	U_{iso}*/U_{eq}
Br1	−0.30053 (4)	0.47161 (2)	0.77208 (2)	0.04456 (8)
O6	−0.2120 (2)	0.27474 (6)	0.73221 (11)	0.0337 (2)
N9	0.4049 (2)	0.18412 (7)	0.42420 (13)	0.0278 (2)
H9	0.529 (3)	0.1816 (10)	0.3639 (18)	0.041 (5)*
N3	0.3696 (2)	0.31647 (6)	0.43388 (13)	0.0288 (2)
N1	0.0413 (3)	0.35239 (6)	0.59830 (14)	0.0293 (2)
H1	−0.035 (4)	0.3873 (9)	0.638 (2)	0.045 (5)*
N7	0.1015 (3)	0.15533 (6)	0.57823 (13)	0.0283 (2)
H7	0.000 (4)	0.1316 (10)	0.6329 (19)	0.044 (5)*
C5	0.1107 (3)	0.22987 (7)	0.57102 (14)	0.0232 (2)
C8	0.2792 (3)	0.12926 (8)	0.48894 (16)	0.0309 (3)
H8	0.312119	0.080303	0.473349	0.037*
C2	0.2315 (3)	0.36593 (8)	0.50019 (16)	0.0309 (3)
H2	0.266402	0.414166	0.478442	0.037*
O1W	−0.7539 (3)	0.60447 (7)	0.73814 (15)	0.0447 (3)
H1W	−0.653 (4)	0.6346 (10)	0.695 (2)	0.067*
H2W	−0.671 (4)	0.5639 (7)	0.741 (2)	0.067*
C4	0.3015 (3)	0.24822 (7)	0.47360 (13)	0.0235 (2)
C6	−0.0384 (3)	0.28405 (7)	0.64259 (14)	0.0245 (2)

Atomic displacement parameters (Å^2)

	U^{11}	U^{22}	U^{33}	U^{12}	U^{13}	U^{23}
Br1	0.05176 (12)	0.02567 (9)	0.06016 (13)	0.00535 (6)	0.02789 (9)	−0.00045 (7)
O6	0.0347 (5)	0.0341 (5)	0.0352 (5)	0.0018 (4)	0.0205 (5)	−0.0004 (4)
N9	0.0272 (5)	0.0312 (6)	0.0267 (5)	0.0032 (4)	0.0122 (5)	−0.0009 (4)
N3	0.0292 (6)	0.0287 (6)	0.0299 (6)	−0.0017 (5)	0.0116 (5)	0.0026 (5)
N1	0.0325 (6)	0.0257 (5)	0.0316 (6)	0.0025 (5)	0.0133 (5)	−0.0016 (5)
N7	0.0311 (6)	0.0251 (5)	0.0301 (6)	−0.0029 (4)	0.0123 (5)	−0.0005 (4)
C5	0.0223 (6)	0.0259 (6)	0.0224 (6)	−0.0010 (5)	0.0072 (5)	−0.0009 (5)
C8	0.0344 (7)	0.0267 (6)	0.0328 (7)	0.0024 (5)	0.0105 (6)	−0.0019 (5)
C2	0.0333 (7)	0.0273 (6)	0.0334 (7)	−0.0011 (5)	0.0103 (6)	0.0033 (5)
O1W	0.0458 (7)	0.0321 (6)	0.0608 (8)	0.0075 (5)	0.0319 (6)	0.0077 (5)
C4	0.0216 (6)	0.0282 (6)	0.0215 (6)	0.0006 (5)	0.0066 (5)	−0.0008 (5)

| C6 | 0.0234 (6) | 0.0285 (6) | 0.0223 (6) | 0.0012 (5) | 0.0060 (5) | −0.0014 (5) |

Geometric parameters (Å, º)

O6—C6	1.2308 (15)	N7—C8	1.3219 (17)
N9—C8	1.3419 (18)	N7—C5	1.3774 (17)
N9—C4	1.3741 (16)	N7—H7	0.849 (14)
N9—H9	0.847 (14)	C5—C4	1.3748 (17)
N3—C2	1.3078 (18)	C5—C6	1.4221 (17)
N3—C4	1.3579 (16)	C8—H8	0.9300
N1—C2	1.3581 (17)	C2—H2	0.9300
N1—C6	1.3879 (17)	O1W—H1W	0.857 (9)
N1—H1	0.840 (14)	O1W—H2W	0.848 (9)
C8—N9—C4	108.32 (10)	N7—C8—N9	109.73 (12)
C8—N9—H9	127.8 (13)	N7—C8—H8	125.1
C4—N9—H9	123.8 (13)	N9—C8—H8	125.1
C2—N3—C4	112.29 (11)	N3—C2—N1	125.15 (13)
C2—N1—C6	125.30 (12)	N3—C2—H2	117.4
C2—N1—H1	119.4 (14)	N1—C2—H2	117.4
C6—N1—H1	115.3 (14)	H1W—O1W—H2W	107.4 (17)
C8—N7—C5	107.98 (11)	N3—C4—N9	127.42 (11)
C8—N7—H7	127.6 (13)	N3—C4—C5	126.22 (12)
C5—N7—H7	124.4 (13)	N9—C4—C5	106.36 (11)
C4—C5—N7	107.61 (11)	O6—C6—N1	122.73 (12)
C4—C5—C6	121.08 (12)	O6—C6—C5	127.31 (13)
N7—C5—C6	131.31 (11)	N1—C6—C5	109.96 (11)
C8—N7—C5—C4	−0.02 (16)	N7—C5—C4—N3	179.07 (12)
C8—N7—C5—C6	179.24 (14)	C6—C5—C4—N3	−0.3 (2)
C5—N7—C8—N9	0.27 (17)	N7—C5—C4—N9	−0.23 (15)
C4—N9—C8—N7	−0.42 (17)	C6—C5—C4—N9	−179.58 (12)
C4—N3—C2—N1	0.2 (2)	C2—N1—C6—O6	179.92 (14)
C6—N1—C2—N3	−0.6 (2)	C2—N1—C6—C5	0.5 (2)
C2—N3—C4—N9	179.41 (14)	C4—C5—C6—O6	−179.46 (14)
C2—N3—C4—C5	0.3 (2)	N7—C5—C6—O6	1.4 (3)
C8—N9—C4—N3	−178.90 (14)	C4—C5—C6—N1	−0.12 (18)
C8—N9—C4—C5	0.39 (16)	N7—C5—C6—N1	−179.30 (14)

Hydrogen-bond geometry (Å, º)

D—H⋯A	D—H	H⋯A	D⋯A	D—H⋯A
N9—H9⋯Br1[i]	0.85 (1)	3.08 (2)	3.5397 (12)	117 (2)
N9—H9⋯O6[i]	0.85 (1)	1.98 (2)	2.7579 (14)	153 (2)
N1—H1⋯Br1	0.84 (1)	2.41 (1)	3.2419 (12)	170 (2)
N7—H7⋯O1W[ii]	0.85 (1)	1.81 (2)	2.6401 (16)	165 (2)
O1W—H1W⋯N3[iii]	0.86 (1)	2.08 (1)	2.9200 (16)	165 (2)

O1*W*—H2*W*⋯Br1	0.85 (1)	2.48 (1)	3.2894 (12)	161 (2)
C8—H8⋯Br1[i]	0.93	2.89	3.4875 (15)	123

Symmetry codes: (i) $x+1$, $-y+1/2$, $z-1/2$; (ii) $-x-1$, $y-1/2$, $-z+3/2$; (iii) $-x$, $-y+1$, $-z+1$.

2,6-Dioxo-2,3,6,9-tetrahydro-1*H*-purin-7-ium bromide monohydrate (II)

Crystal data

$C_5H_5N_4O_2{}^+\cdot Br^-\cdot H_2O$	$F(000) = 496$
$M_r = 251.06$	$D_x = 2.021$ Mg m^{-3}
Monoclinic, $P2_1/c$	Mo $K\alpha$ radiation, $\lambda = 0.71073$ Å
$a = 4.9225$ (2) Å	Cell parameters from 1418 reflections
$b = 22.7572$ (17) Å	$\theta = 2.9$–29.6°
$c = 7.5601$ (5) Å	$\mu = 4.96$ mm^{-1}
$\beta = 103.003$ (3)°	$T = 303$ K
$V = 825.18$ (9) Å^3	Plate, colourless
$Z = 4$	$0.55 \times 0.37 \times 0.31$ mm

Data collection

Bruker APEXII CCD diffractometer	1855 independent reflections
	1418 reflections with $I > 2\sigma(I)$
φ and ω scans	$R_{int} = 0.045$
Absorption correction: multi-scan (SADABS; Bruker, 2016)	$\theta_{max} = 29.7°$, $\theta_{min} = 2.9°$
	$h = -6 \rightarrow 6$
$T_{min} = 0.316$, $T_{max} = 0.561$	$k = -30 \rightarrow 30$
5810 measured reflections	$l = -9 \rightarrow 9$

Refinement

Refinement on F^2	Secondary atom site location: difference Fourier map
Least-squares matrix: full	
$R[F^2 > 2\sigma(F^2)] = 0.036$	Hydrogen site location: difference Fourier map
$wR(F^2) = 0.080$	Only H-atom coordinates refined
$S = 1.10$	$w = 1/[\sigma^2(F_o^2) + (0.0151P)^2 + 1.7175P]$
1855 reflections	where $P = (F_o^2 + 2F_c^2)/3$
139 parameters	$(\Delta/\sigma)_{max} < 0.001$
9 restraints	$\Delta\rho_{max} = 0.42$ e Å^{-3}
Primary atom site location: structure-invariant direct methods	$\Delta\rho_{min} = -0.62$ e Å^{-3}

Special details

Geometry. All esds (except the esd in the dihedral angle between two l.s. planes) are estimated using the full covariance matrix. The cell esds are taken into account individually in the estimation of esds in distances, angles and torsion angles; correlations between esds in cell parameters are only used when they are defined by crystal symmetry. An approximate (isotropic) treatment of cell esds is used for estimating esds involving l.s. planes.

Fractional atomic coordinates and isotropic or equivalent isotropic displacement parameters (Å²)

	x	*y*	*z*	$U_{iso}*/U_{eq}$
Br1	−0.16454 (8)	0.20412 (2)	0.47569 (6)	0.03200 (14)
O6	0.8033 (5)	0.47823 (12)	0.6033 (4)	0.0318 (6)
C6	0.6301 (7)	0.44615 (16)	0.6465 (5)	0.0241 (8)
N1	0.5267 (7)	0.45642 (14)	0.7988 (4)	0.0273 (7)
H1	0.578 (8)	0.4867 (13)	0.855 (5)	0.033*

C2	0.3313 (8)	0.42399 (16)	0.8628 (5)	0.0254 (8)
O2	0.2541 (6)	0.43894 (13)	0.9992 (4)	0.0380 (7)
N3	0.2278 (6)	0.37489 (13)	0.7647 (4)	0.0251 (7)
H3	0.126 (7)	0.3545 (16)	0.812 (5)	0.030*
C4	0.3212 (7)	0.36166 (15)	0.6147 (5)	0.0238 (8)
C5	0.5108 (7)	0.39456 (16)	0.5538 (5)	0.0237 (8)
N7	0.5509 (7)	0.36852 (14)	0.3972 (4)	0.0273 (7)
H7	0.651 (8)	0.3804 (18)	0.332 (5)	0.033*
C8	0.3919 (8)	0.32168 (18)	0.3652 (6)	0.0304 (9)
H8	0.384 (9)	0.2947 (18)	0.265 (6)	0.036*
N9	0.2477 (7)	0.31597 (14)	0.4956 (5)	0.0279 (7)
H9	0.148 (7)	0.2876 (14)	0.503 (6)	0.033*
O1W	0.8947 (7)	0.42353 (14)	0.2374 (4)	0.0434 (8)
H1WA	0.983 (9)	0.4523 (16)	0.298 (6)	0.065*
H1WB	0.980 (9)	0.415 (2)	0.154 (5)	0.065*

Atomic displacement parameters (Å^2)

	U^{11}	U^{22}	U^{33}	U^{12}	U^{13}	U^{23}
Br1	0.0307 (2)	0.0253 (2)	0.0413 (2)	−0.00152 (17)	0.01087 (16)	−0.00286 (18)
O6	0.0317 (15)	0.0309 (15)	0.0360 (16)	−0.0110 (12)	0.0147 (13)	−0.0028 (12)
C6	0.0231 (18)	0.0217 (18)	0.028 (2)	−0.0001 (14)	0.0057 (16)	0.0046 (15)
N1	0.0294 (17)	0.0253 (17)	0.0292 (19)	−0.0097 (14)	0.0111 (15)	−0.0046 (14)
C2	0.0255 (19)	0.0224 (19)	0.029 (2)	−0.0030 (15)	0.0079 (17)	0.0042 (16)
O2	0.0431 (17)	0.0432 (18)	0.0338 (17)	−0.0118 (14)	0.0216 (14)	−0.0079 (14)
N3	0.0246 (16)	0.0232 (16)	0.0305 (18)	−0.0041 (12)	0.0128 (14)	0.0050 (13)
C4	0.0236 (18)	0.0193 (17)	0.027 (2)	0.0011 (14)	0.0028 (15)	0.0039 (15)
C5	0.0231 (18)	0.0246 (18)	0.0232 (19)	−0.0018 (14)	0.0050 (15)	−0.0008 (15)
N7	0.0291 (17)	0.0286 (17)	0.0265 (18)	−0.0023 (14)	0.0109 (14)	0.0005 (14)
C8	0.035 (2)	0.028 (2)	0.028 (2)	−0.0013 (17)	0.0051 (18)	−0.0048 (17)
N9	0.0299 (17)	0.0186 (15)	0.0346 (19)	−0.0040 (13)	0.0061 (15)	0.0000 (14)
O1W	0.0484 (19)	0.0449 (19)	0.046 (2)	−0.0199 (15)	0.0290 (16)	−0.0172 (15)

Geometric parameters (Å, º)

O6—C6	1.221 (4)	C4—N9	1.370 (5)
C6—N1	1.380 (5)	C5—N7	1.378 (5)
C6—C5	1.425 (5)	N7—C8	1.312 (5)
N1—C2	1.383 (5)	N7—H7	0.82 (2)
N1—H1	0.82 (2)	C8—N9	1.344 (5)
C2—O2	1.224 (5)	C8—H8	0.97 (4)
C2—N3	1.374 (5)	N9—H9	0.82 (2)
N3—C4	1.350 (5)	O1W—H1WA	0.857 (10)
N3—H3	0.82 (2)	O1W—H1WB	0.860 (10)
C4—C5	1.355 (5)		
O6—C6—N1	122.2 (3)	C5—C4—N9	107.2 (3)
O6—C6—C5	126.6 (4)	C4—C5—N7	107.3 (3)

N1—C6—C5	111.2 (3)	C4—C5—C6	121.8 (3)
C6—N1—C2	128.1 (3)	N7—C5—C6	130.9 (3)
C6—N1—H1	116 (3)	C8—N7—C5	108.2 (3)
C2—N1—H1	115 (3)	C8—N7—H7	125 (3)
O2—C2—N3	122.2 (3)	C5—N7—H7	127 (3)
O2—C2—N1	121.2 (3)	N7—C8—N9	109.6 (4)
N3—C2—N1	116.6 (3)	N7—C8—H8	125 (3)
C4—N3—C2	118.7 (3)	N9—C8—H8	125 (3)
C4—N3—H3	126 (3)	C8—N9—C4	107.7 (3)
C2—N3—H3	115 (3)	C8—N9—H9	123 (3)
N3—C4—C5	123.6 (3)	C4—N9—H9	129 (3)
N3—C4—N9	129.2 (3)	H1WA—O1W—H1WB	107 (2)
O6—C6—N1—C2	179.8 (4)	N9—C4—C5—C6	179.6 (3)
C5—C6—N1—C2	−0.7 (5)	O6—C6—C5—C4	179.3 (4)
C6—N1—C2—O2	−178.6 (4)	N1—C6—C5—C4	−0.1 (5)
C6—N1—C2—N3	0.8 (6)	O6—C6—C5—N7	−1.2 (7)
O2—C2—N3—C4	179.3 (4)	N1—C6—C5—N7	179.3 (4)
N1—C2—N3—C4	−0.1 (5)	C4—C5—N7—C8	−0.1 (4)
C2—N3—C4—C5	−0.6 (5)	C6—C5—N7—C8	−179.6 (4)
C2—N3—C4—N9	−179.3 (4)	C5—N7—C8—N9	0.1 (5)
N3—C4—C5—N7	−178.8 (3)	N7—C8—N9—C4	0.0 (4)
N9—C4—C5—N7	0.1 (4)	N3—C4—N9—C8	178.7 (4)
N3—C4—C5—C6	0.8 (6)	C5—C4—N9—C8	−0.1 (4)

Hydrogen-bond geometry (Å, º)

D—H⋯A	D—H	H⋯A	D⋯A	D—H⋯A
N1—H1⋯O2[i]	0.82 (2)	2.09 (2)	2.903 (4)	175 (4)
N3—H3⋯Br1[ii]	0.82 (2)	2.48 (2)	3.301 (3)	176 (4)
N7—H7⋯O1W	0.82 (2)	1.81 (2)	2.609 (4)	163 (4)
N9—H9⋯Br1	0.82 (2)	2.43 (2)	3.237 (3)	172 (4)
O1W—H1WA⋯O6[iii]	0.86 (1)	1.95 (1)	2.802 (4)	171 (5)
O1W—H1WB⋯Br1[iv]	0.86 (1)	3.03 (4)	3.490 (3)	115 (3)
O1W—H1WB⋯O2[v]	0.86 (1)	2.05 (3)	2.816 (4)	149 (4)

Symmetry codes: (i) −x+1, −y+1, −z+2; (ii) x, −y+1/2, z+1/2; (iii) −x+2, −y+1, −z+1; (iv) x+1, −y+1/2, z−1/2; (v) x+1, y, z−1.

Percentage of non-covalent interaction in supramolecular packing analyzed by Hirshfeld surface analysis

CONTACT	SALT (I)	SALT (II)
H⋯Br /Br⋯H	22.3%	25.4%
O⋯H/H⋯O	19.7%	23.4%
H⋯N/N⋯H	13.5%	7.5%
C⋯H/H⋯C	6.4%	9.6%
H⋯H	23.4%	15.9%